

1 **Title:** Surface-Parallel Sensor Orientation for Assessing Energy Balance  
2 Components on Mountain Slopes  
3 **Author(s):** Serrano-Ortiz, P.; Sánchez-Cañete, E.P.; Olmo, F.J.; et al.  
4 **Source:** Boundary-Layer Meteorology **Volume:** 158 **Issue:** 3 **Pages:** 489-  
5 499 **Published:** 2016  
6 **DOI:** 10.1007/s10546-015-0099-4  
7

# 8 Surface-parallel sensor orientation for assessing energy 9 balance components on mountain slopes

10  
11 P. Serrano-Ortiz, E. P. Sánchez-Cañete, F. J. Olmo, S. Metzger, O. Pérez-Priego, A.  
12 Carrara, L. Alados-Arboledas, and A. S. Kowalski

13  
14 Received: DD Month YEAR/ Accepted: DD Month YEAR

15  
16 Abstract The consistency of eddy-covariance measurements is often evaluated in terms  
17 of the degree of energy balance closure. Even over sloping terrain, instrumentation for  
18 measuring energy balance components are commonly installed horizontally, i.e.  
19 perpendicular to the geo-potential gradient. Subsequently, turbulent fluxes of sensible  
20 and latent heat are rotated perpendicular to the mean streamlines using tilt correction  
21 algorithms. However, net radiation ( $R_n$ ) and soil heat fluxes ( $G$ ) are treated differently,  
22 and typically only  $R_n$  is corrected to account for slope. With an applied case study, we  
23 show and argue several advantages of installing sensors surface-parallel to measure  
24 surface-normal  $R_n$  and  $G$ . For a 17% southwest-facing slope, our results show that  
25 horizontal installation results in hysteresis in the energy balance closure and errors of up  
26 to 25%. Finally, we propose an approximation to estimate surface-normal  $R_n$ , when only  
27 vertical  $R_n$  measurements are available.

28  
29 **Keywords** Energy balance closure • Hysteresis • Net radiation• Soil heat flux • Sloping  
30 terrains

31  
32 P. Serrano-Ortiz  
33 Departamento de Ecología, Universidad de Granada, Granada, 18071, Spain.  
34 e-mail: penelope@ugr.es

35  
36 P. Serrano-Ortiz·E. P. Sánchez-Cañete·F. J. Olmo·L. Alados-Arboledas·A. S. Kowalski  
37 Andalusian Institute for Earth System Research (CEAMA-IISTA), Universidad de Granada, 18006, Spain.

38  
39 E. P. Sánchez-Cañete  
40 B2 Earthscience, Biosphere 2, University of Arizona, Tucson, AZ 85721, USA

41  
42 F. J. Olmo·L. Alados-Arboledas·A. S. Kowalski  
43 Departamento de Física Aplicada, Universidad de Granada, Granada, 18071, Spain.

44  
45 S. Metzger  
46 National Ecological Observatory Network (NEON), Boulder, USA  
47 Institute for Arctic and Alpine Research, University of Colorado, Boulder, USA.

48  
49 O. Pérez-Priego  
50 Department of Biogeochemical Integration, Max Planck Institute for Biogeochemistry, Jena, 07745, Germany.

51  
52 A. Carrara  
53 Fundación Centro de Estudios Ambientales del Mediterráneo (CEAM), Valencia, 46980, Spain.

## 55 **1 Introduction**

56 Measurements of turbulent fluxes in varying environments are one of the tools scientists  
57 and decision makers rely on for assessing and forecasting global warming (Kaminski et  
58 al. 2012, Koffi et al. 2013). Thus, eddy-covariance towers have proliferated around the  
59 world in the last two decades (FLUXNET tower network; Baldocchi et al. 2001). Since  
60 ideal sites are rarely found worldwide, there was a great need to extend the applicability  
61 of the eddy-covariance method to situations over non-ideal (or “complex”) terrain.  
62 Different studies even concluded that the eddy-covariance method can be used over  
63 sloping terrain to evaluate energy and CO<sub>2</sub>/H<sub>2</sub>O fluxes of whole ecosystems (Hammerle  
64 et al. 2007, Hiller et al. 2008). However, general problems of the eddy-covariance  
65 method are aggravated by sloping terrain. Both the error induced by neglecting vertical  
66 and horizontal advective fluxes (Aubinet et al. 2003, Aubinet et al. 2005) and the  
67 underestimation of night-time ecosystem respiration during stable night-time conditions  
68 (Gu et al. 2005, Aubinet 2008) depend critically on slope, although such problems are  
69 less pronounced over short vegetation.

70         One of the most commonly used methods for evaluating the consistency of eddy-  
71 covariance turbulent flux measurements is to assess closure of the energy balance  
72 (Wilson et al. 2002, Stoy et al. 2013). This quality control criterion for eddy-covariance  
73 measurements consists of comparing the sum of the latent ( $LE$ ) and sensible ( $H$ ) heat  
74 fluxes, measured with the eddy-covariance method, to the available energy consisting of  
75 net radiation ( $R_n$ ) minus the soil heat flux ( $G$ ). According to the first law of  
76 thermodynamics, incoming and outgoing energy components must balance one another.  
77 This independent assessment of eddy-covariance measurement reliability has been  
78 evaluated for many FLUXNET sites with a mean imbalance on the order of 20%  
79 (Wilson et al. 2002). The reasons for the general imbalance remain unclear and are  
80 under discussion (Foken 2008, Leuning et al. 2012, Stoy et al. 2013), and turbulent  
81 fluxes are often considered “acceptable” when the energy balance residual does not  
82 exceed 30%. Over sloping terrain, the energy budget quality control yields results  
83 comparable to those for sites located in more ideal terrain (Hammerle et al. 2007, Hiller  
84 et al. 2008, Etzold et al. 2010). In the following, we focus on ecosystem-scale  
85 exchanges over a mountain slope that is quasi-uniform across and beyond the source  
86 area (footprint) of the flux measurements. That is, we focus on the effect of the average

87 slope over scales of hectares on the energy balance. Smaller undulations that can even  
88 exist within flat terrain (such as ploughed farmlands) are not the subject of this study  
89 and are addressed elsewhere (Wohlfahrt and Tasser 2014).

90 Overall, the goal of an energy balance study must be to represent all contributing  
91 terms in the same way that they influence the exchange surface. This can be achieved by  
92 minimizing the incident angle between a contributing term and its measurement  
93 regardless of the exchange surface orientation. Atmospheric turbulence results in down-  
94 gradient transport by turbulent diffusion, with the “exchange” coordinate of the scalar  
95 flux being perpendicular to the streamlines/surface. For radiation components, both the  
96 irradiance and emittance relevant to the surface are clearly in the normal direction,  
97 irrespective of the geopotential gradient (this is why solar panels are not installed  
98 horizontally). Such net radiative effects also establish isotherms parallel to the surface  
99 and soil temperature gradients in the surface-normal direction, which is therefore the  
100 relevant direction to measure  $G$ .

101 Over sloping sites, eddy-covariance systems are typically installed horizontally  
102 and the resulting fluxes  $H$  and  $LE$  are subsequently rotated perpendicular to the mean  
103 streamlines. However, the  $R_n$  and  $G$  terms contributing to the energy balance are treated  
104 differently. Net radiometers are installed horizontally and either (a) no rotation is  
105 applied (e.g., Etzold et al. 2010) or (b) the incoming solar radiation component of the  
106 net radiation is corrected for the inclination, arguing that this is the most important  
107 component contributing to  $R_n$  (Matzinger et al. 2003, Hammerle et al. 2007, Hiller et al.  
108 2008, Saitoh et al. 2011). Oftentimes no information is provided on the alignment of the  
109  $R_n$  and  $G$  sensors.

110 This study examines the advantages of installing the net radiometer and soil heat flux  
111 instruments parallel to the average slope. Section 2 provides information on the study  
112 site and the sensor deployments. In Sect. 3, we present the case study results of  
113 horizontal vs. parallel sensor installations, and propose an approximation to estimate  
114 surface-normal  $R_n$ , when only vertical  $R_n$  measured with horizontally oriented (i.e.,  
115 level) sensors is available. Finally, in Sect. 4 and 5 we discuss our findings and provide  
116 concluding recommendations.

117

## 118 **2 Methods**

### 119 **2.1 Site description**

120 The experimental part of the study was conducted in the Sierra Nevada National Park in  
121 south-eastern Spain (36°58'3.68''N; 3°28'37.04''W, 2320 m a.s.l.; Fig 1). Vegetation  
122 consists of grass and forbs (*Genista versicolor*, *Festuca spp.* and *Sesamoidesprostata*,  
123 dominant species) recovering in the wake of a 2005 wildfire. Given the short vegetation  
124 and the aerodynamically simple surface, the contribution of air storage to net exchanges  
125 is very small and thus neglected (Suyker and Verma 2001, Kowalski et al. 2003). An  
126 eddy covariance tower was installed in 2009 over an averaged slope of 17% of  
127 southwest (255°) aspect. Previous studies showed that fluxes typically originate from  
128 source areas within approximately 300 m of the tower (Serrano-Ortiz et al. 2011).

129

### 130 **2.2 Sensor deployments**

131 The following analyses were performed on data from 7 July to 20 August of 2010, with  
132 34 days under cloud-free conditions and 10 partially cloudy days; no fully overcast  
133 conditions occurred. During this period the eddy-covariance tower measured turbulent  
134 exchanges of energy between the surface and the atmosphere. Sensible ( $H$ ) and latent  
135 ( $LE$ ) heat fluxes were calculated from fast-response (10 Hz) instruments (Infrared gas  
136 analyser Li-7500, Lincoln, NE, USA; three-axis sonic anemometer Model 81000, R.M.  
137 Young, Traverse City, MI, USA; mounted horizontally so that "w" represents the  
138 vertical wind; valid operating range for attack angle in the range  $\pm 60^\circ$ ) mounted atop a  
139 6-m tower.

140 Means, variances and covariances were calculated for half-hour periods following  
141 Reynolds' rules, and eddy flux corrections for density perturbations (Webb et al. 1980)  
142 and tests for stationarity and turbulence development tests were applied using the  
143 EddyPro 5.1.1 software. The stationarity test compares the covariances determined for  
144 the half hourly period and for shorter intervals within this period (usually 5 minutes). A  
145 time series is considered to be steady state if the difference between both covariances is  
146 lower than 30% (Mauder and Foken 2004). The turbulence development was tested by  
147 using the so-called flux-variance similarity where the ratio of the standard deviation of a  
148 turbulent parameter and its turbulent flux (measured parameter) is a function of the  
149 stability (modelled parameter). Well developed turbulence can be assumed if the  
150 difference between the measured and the modelled parameter is lower than 30%

151 (Mauder and Foken 2004). After applying both tests, the EddyPro 5.1.1 software  
152 provides the flag “0” for high quality fluxes (differences <30% for both test), “1” for  
153 intermediate quality fluxes (differences <30% for one test) and “2” for poor quality  
154 fluxes (differences >30% for both test).

155 Since no systematic error has been observed for applying different rotation methods  
156 over sloped sites (e.g., Turnipseed et al. 2003, Shimizu 2015) and particularly for our  
157 experimental site (double rotation vs planar fit showed no significant differences, data  
158 not shown), the double coordinate rotation was used to ensure that the rotated average  
159 "w" is zero in the direction normal to the surface. While double rotation of half hourly  
160 data is one of the most common methods used, it is frequently cited inadequately: the  
161 often-cited paper by McMillen (1988) relied on erroneous equations from a grey-  
162 literature report by Tanner and Thurtell (1969). The correct version was first provided  
163 by Kowalski et al. (1997) and is now also frequently cited via Aubinet et al. (2000).

164 In addition to the turbulent fluxes, available energy was determined by duplicate  
165 sensors in two configurations, one parallel to the surface and the other horizontal. For  
166 each, a net radiometer (NR Lite, Kipp&Zonen, Delft, Netherlands) was located 2 m  
167 above the surface, and two heat flux plates (HFP01SC, Hukseflux, Delft, Netherlands)  
168 were installed at 8 cm depth, with two pairs of soil temperature probes (TCAV,  
169 Campbell Scientific, Logan, UT, USA) at 2 and 6 cm depth, and a water content  
170 reflectometer (CS616, Campbell Scientific, Logan, UT, USA) at 4 cm depth. The soil  
171 heat flux ( $G$ ) was calculated by adding the measured heat flux at a fixed depth (8 cm)  
172 under bare soil to the energy stored in the layer above the heat flux plates, based on the  
173 specific heat capacity of the soil and changes in the temperature and soil water content  
174 with time (Massman 1992, Domingo et al. 2000). Finally, the incident and reflected  
175 photosynthetic photon flux densities (PPFD) were measured by quantum sensors (Li-  
176 190, Lincoln, NE, USA) to identify the partially cloudy days and estimate the surface  
177 albedo.

178

### 179 **2.3 Modelling**

180 Following Olmo et al. (1999), the surface-normal  $R_n$  was modelled based on vertical  $R_n$   
181 measurements. First, vertical daytime  $R_n$  values were converted to global irradiance  
182 ( $R_g$ ), defined as the total amount of shortwave radiation (direct+diffuse;  $W m^{-2}$ ) received  
183 from above by a surface (Iqbal 1983), using the linear relationship between  $R_n$  and  $R_g$   
184 evaluated by Alados et al. (2003) for semi-arid sites:

185 
$$R_n = a R_g + b, \quad (1)$$

186 where  $a=0.709$  and  $b=-25.4 \text{ W m}^{-2}$ .

187 Secondly, the daytime surface-normal  $R_g$  was modelled following Olmo et al.  
188 (1999)

189 
$$R_{g\psi} = R_g \exp(-k_t(\psi^2 - \theta_z^2)) F_c \quad (\text{day}) \quad (2)$$

190 where  $R_{g\psi}$  is the global irradiance on the inclined surface,  $R_g$  is the global irradiance on  
191 the horizontal surface,  $\psi$  is the angular distance (in radians) from the surface normal to  
192 the sun's position,  $\theta_z$  denotes the solar zenith angle,  $k_t$  is the clearness index,  $F_c$  is a  
193 multiplying factor to take into account anisotropic reflections.

194 The angular distance  $\psi$  can be evaluated as follows:

195 
$$\cos \psi = \sin \alpha \sin \alpha_s + \cos \alpha \cos \alpha_s \cos(\varphi_s - \varphi), \quad (3)$$

196 where  $\alpha$  is the angle of the slope (surface elevation) with respect to the horizontal  
197 surface,  $\alpha_s$  is the sun elevation angle with respect to the horizontal surface,  $\varphi_s$  is the sun  
198 azimuth and  $\varphi$  the surface azimuth (Fig. 2).

199 The clearness index can be evaluated as follows:

200 
$$K_t = R_g / R_{g\text{ext}}, \quad (4)$$

201 where  $R_{g\text{ext}}$  is the extraterrestrial irradiance calculated as follow (Iqbal, 1983):

202 
$$R_{g\text{ext}} = I_{sc} (r_0/r)^2 \cos \theta_z, \quad (5)$$

203 where  $I_{sc}$  is the solar constant ( $1367 \text{ W m}^{-2}$ ),  $r_0$  is the average sun-earth distance and  $r$  is  
204 the real sun-earth distance according to day of year.

205 Concerning the anisotropic correction factor,  $F_c$ , we have tested various types of  
206 functions and obtained the best agreement between the computed and observed  
207 radiation values as follows:

208 
$$F_c = \sin \psi / (0.55 - \rho), \quad (6)$$

209 where  $\rho$  is the surface albedo, approximated as the ratio of the averaged daytime  
210 reflected to incident PPFD for the studied period ( $\rho = 0.12$ ).

211 Thirdly, the obtained results were converted into surface-normal  $R_n$  values  
212 ( $R_{n\psi}$ ), using again the site-specific linear regression (1). Finally, the nighttime values of  
213 surface-normal  $R_n$  were directly modelled as follow:

214 
$$R_{n\psi} = R_n \cos \alpha_s. \quad (7)$$

215 In contrast to the  $R_n$  measurement, the vector components of the soil heat flux are not  
216 known. Also, unlike the turbulence sensors the soil heat flux plate measures only along

217 a single axis. Consequently, no correction was attempted for transforming vertical  $G$   
218 into a surface-normal coordinate.

219

### 220 **3 Results**

221 Data are reported using Coordinated Universal Time (UTC), which leads local solar  
222 time at this site by less than 15 minutes.

223 For our study case, vertical  $R_n$  and  $G$  measured with horizontal sensor  
224 orientation underestimate available energy due to the slight southern aspect of the slope,  
225 with the expected delay in the maxima due to the predominantly western aspect (Fig.  
226 3a). Significant differences between morning and afternoon values and daily totals of  $R_n$   
227 and  $G$  were measured comparing both orientations. The radiometer installed  
228 horizontally overestimated morning  $R_n$  by around  $100 \text{ Wm}^{-2}$  and underestimated  
229 afternoon values by around  $150 \text{ Wm}^{-2}$ , resulting in 21% and 16% underestimation of the  
230 daily means under cloud-free and partially cloudy conditions respectively (Fig. 3).  
231 Similarly, horizontally installed soil heat flux plates overestimated morning values by  
232 around  $25 \text{ Wm}^{-2}$  and underestimated afternoon values by  $40 \text{ Wm}^{-2}$ , leading to an overall  
233 underestimation of 13% in the daily totals under cloud free conditions; no  
234 underestimation was observed under partially cloudy conditions (Fig. 3c).

235 This results in clear hysteresis in energy balance closure when vertical  $R_n$  and  $G$   
236 values from horizontal sensors were used (Fig. 4a and 5a). Maximum values of vertical  
237  $R_n$  and  $G$  were measured at noon, whereas for rotated  $H$  and  $LE$  peaks occurred in late  
238 afternoon (Figure 5a). The situation is resolved when sensors are installed parallel to  
239 the slope measuring surface-normal  $R_n$  and  $G$ . Peak values of all components of the  
240 energy balance occurred in late afternoon, in accordance with the south-western aspect  
241 of the slope (Fig. 5f), improving both the slope (from 1.20 to 1.06; Fig. 4f) and the  
242 explained variance ( $R^2$  from 0.83 to 0.99; Fig 4f) of the linear least-squares regression.  
243 When vertical  $G$  is measured with horizontal sensor orientation (Fig. 5c), the energy  
244 balance closure (regression slope) does not change substantially, but scatter of around  
245  $100 \text{ Wm}^{-2}$  increases (Fig. 4c). When the modelled surface-normal  $R_n$  is used (Fig 5b and  
246 e), the regression fit is also improved ( $R^2=0.92$ ; Fig. 4b and e). Note that, despite the  
247 good match between measured and modelled surface-normal  $R_n$  (slope= $1.009 \pm 0.005$ , y-  
248 intercept= $-2 \pm 1$ ,  $R^2=0.96$ ;  $n=1983$ ), the comparison of daily patterns shows clear  
249 mismatches at sunrise, sunset and midday (Fig. 3). Under cloud-free conditions (Fig. 3a)

250 modelled surface-normal  $R_n$  overestimated sunrise and midday values by around 70  
251  $\text{Wm}^{-2}$  and similarly underestimated sunset values. Under partially cloudy conditions  
252 (Fig. 3c), modelled surface-normal  $R_n$  yielded clearly overestimated values from 0900  
253 to 1700 UTC by up to  $135 \text{ Wm}^{-2}$ . This results in a deviation from the energy balance  
254 closure 1:1 line between  $100 \text{ Wm}^{-2}$  and  $300 \text{ Wm}^{-2}$  when considering the whole database  
255 (Fig. 4b, 4e), and 6% underestimation and 20% overestimation in the daily mean for  
256 sunny and partially cloudy days respectively (Fig. 3a and c).

257

## 258 **4 Discussion**

259 Our case study confirms improved energy balance closure when both the net radiometer  
260 and soil heat flux instruments were installed parallel to the slope compared to other  
261 configurations, such as horizontal or modelled normal-surface  $R_n$ . For the case of  $G$ ,  
262 with modest contribution to the energy balance, parallel installation did not substantially  
263 improve the slope, but did reduce the scatter. It needs to be considered that  $G$   
264 measurements only represent their immediate environment (of order  $0.01 \text{ m}^2$ ) whereas  
265 radiation and turbulent flux measurements represent of order  $100 \text{ m}^2$  and  $1000 \text{ m}^2$ ,  
266 respectively, for these measurement heights. Hence, for representing a spatial scale  
267 more comparable to the radiation and flux measurements, a population of soil plates  
268 placed parallel to the average slope is required.

269 Since  $R_n$  represents more than 70% of available energy, it is commonly accepted  
270 by the FLUXNET community to install radiometers horizontally and approximate  
271 surface-normal  $R_n$  following trigonometric corrections in post-processing, but to neglect  
272 the effect of the slope on  $G$  (Hammerle et al. 2007, Hiller et al. 2008, Zitouna-Chebbi et  
273 al. 2012). If such an approximation is to be performed reliably, not only net radiometers  
274 but also pyranometers should be installed to distinguish the total, direct and diffuse  
275 shortwave radiation components. In such a way, direct shortwave radiation can be easily  
276 corrected for slope effects knowing the azimuthal and elevation angles, latitude and  
277 surface inclination (Garnier and Ohmura 1968, Whiteman et al. 1989). Since direct  
278 shortwave radiation represents from 60 to 80% of  $R_n$  for mid-latitudes, and is the  
279 component most affected by slope effects (Holst et al. 2005), such post-processing  
280 correction typically yields acceptable results. However, according to Oliver (1992),  
281 under partially cloudy conditions, information about cloud cover and opacity is required  
282 and the correction quickly becomes either complex or inaccurate. Moreover, not only

283 the direct but also the reflected shortwave radiation component (from 5 to 15% of the  
284 total  $R_n$ ) is affected by the slope (Holst et al. 2005). Additionally, our results show that,  
285 under cloud-free conditions, approximating surface-normal  $R_n$  is justified when stations  
286 measure only  $R_n$  and not its components. However, under partially cloudy conditions the  
287 model clearly overestimated  $R_n$ . Unfortunately, fully overcast conditions were lacking  
288 during our experiment, and we cannot evaluate the model performance on cloudy days.  
289 Furthermore, a site-specific linear regression relationship is required as an intermediate  
290 step to convert the measured  $R_n$  into global irradiance and vice versa.

291 While in the immediate air layer above an exchange surface, net-transport is down-  
292 gradient, i.e. surface-normal, there are also relevant cases for examining vertical  
293 exchange of heat: with increasing distance from the exchange surface, some types of  
294 atmospheric flows are dominated by buoyancy. In this case the relevant direction of  
295 transport is vertical, following the geopotential gradient. For example, when studying  
296 atmospheric stability, the vertical exchange of heat (or actually: buoyancy) must be  
297 considered. This implies the need to consider vertical buoyancy fluxes when calculating  
298 the Richardson number, for example, irrespective of surface orientation.

299

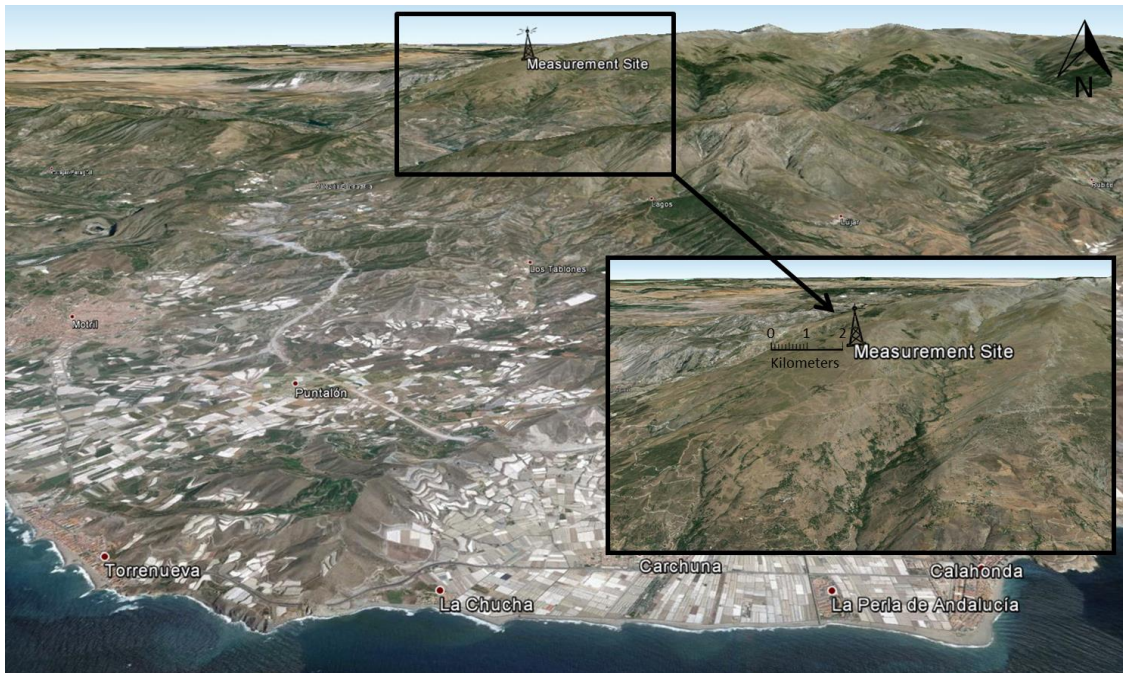
## 300 **5 Conclusion and recommendations**

301 For energy balance studies the transport direction of interest is surface-normal.  
302 Consequently, for assessing the energy balance over a sloping surface without complex  
303 local topography or undulations, we recommend installing the net radiometer and soil  
304 heat flux plates parallel to the average slope. For other uses, such as validation of  
305 regional models using the energy fluxes measured at the ecosystem scale, spatial  
306 aggregation beyond differing definitions of the exchange direction needs to be  
307 considered. Equally important, slope and aspect lead to distinct differences in the  
308 ecosystem types, necessitating a careful evaluation of spatial representativeness of the  
309 measured fluxes.

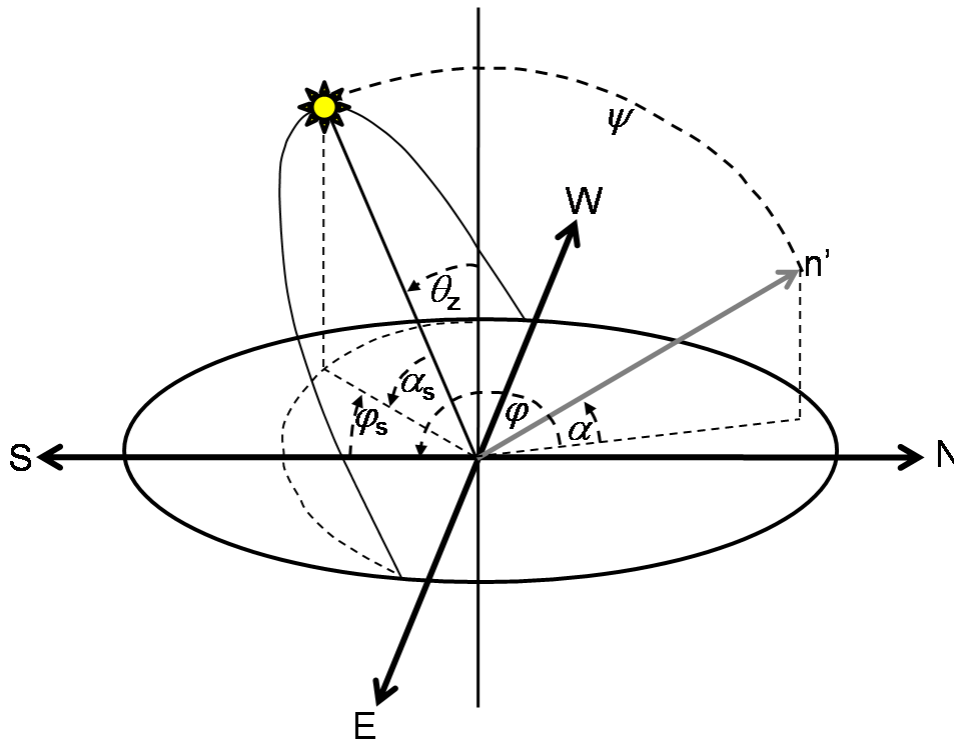
310

311

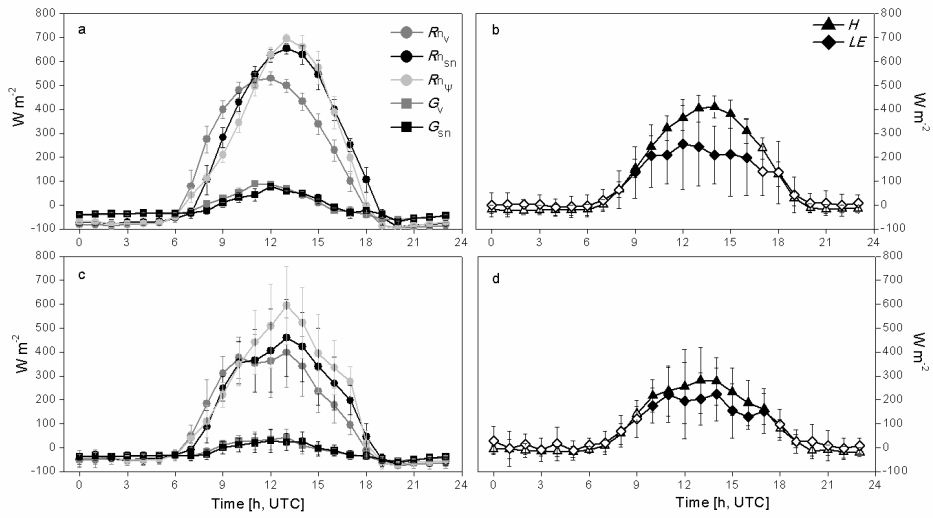
312 **Figures**



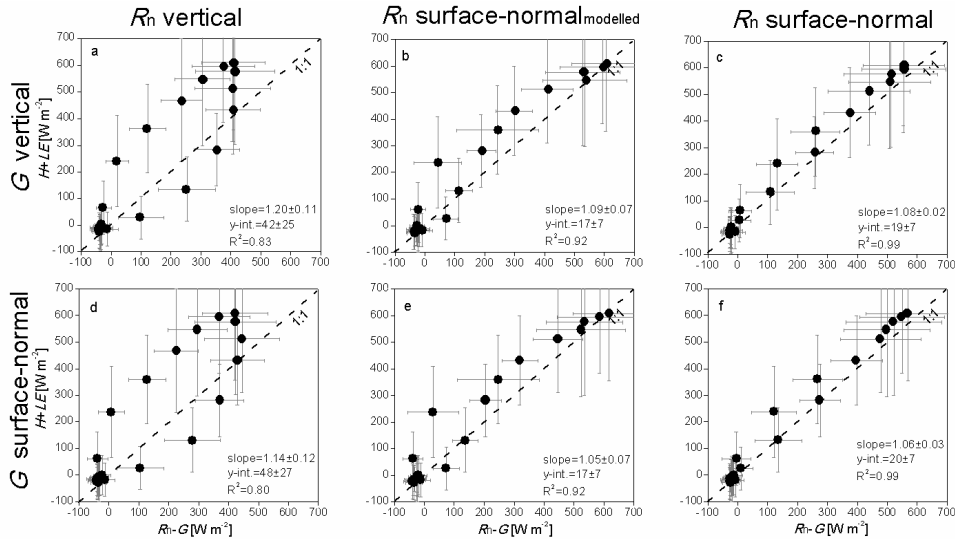
313  
 314 **Fig 1** Measurement site on the south-western slope of the Sierra Nevada National Park, Spain (Tower not  
 315 to scale.). Source: Google Earth, 36°58'3.68"N; 3°28'37.04"W, image: Landsat, imagery date August 4,  
 316 2012, accessed November 9, 2014.



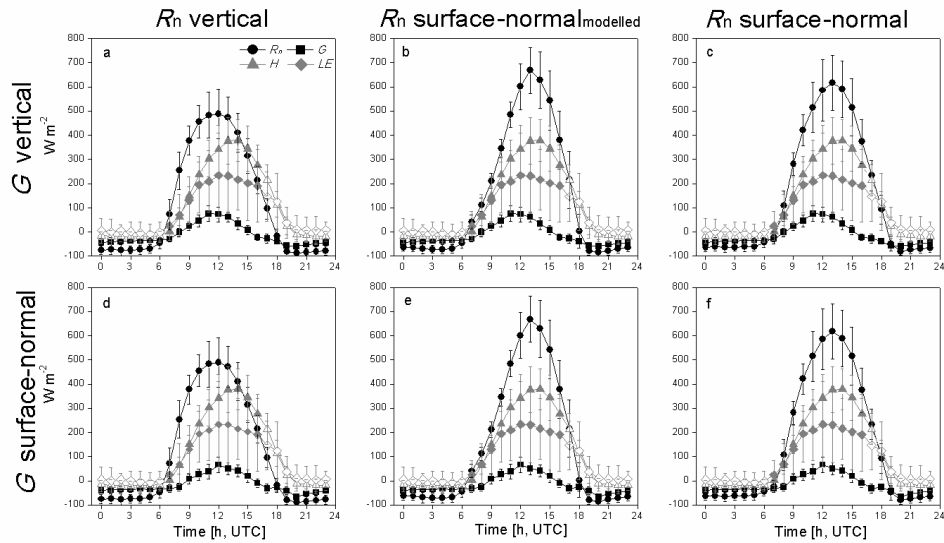
317  
 318 **Fig 2** Sketch of the angles involved in the radiation model. Angular distance (in radians) from the surface  
 319 normal ( $n'$ ) to the sun's position ( $\psi$ ); solar zenith angle ( $\theta_z$ ); angle of the slope (surface elevation) with  
 320 respect to the horizontal surface ( $\alpha$ ), sun elevation angle respect to the horizontal surface ( $\alpha_s$ ), sun  
 321 azimuth ( $\varphi_s$ ), surface azimuth ( $\varphi$ ).



323  
 324 **Fig 3** Daily patterns of the energy balance components under cloud-free (a, b) and partially cloudy (c, d)  
 325 conditions. Vertical radiation ( $R_n$ ) and soil heat flux ( $G$ ) measured with horizontal sensor orientation  
 326 (subscript "v"; dark gray symbols), surface-normal  $R_n$  and  $G$  measured with surface-parallel sensor  
 327 orientation (subscript "sn"; black symbols) and modelled surface-normal  $R_n$  (subscript " $\psi$ "; light gray  
 328 circles) for panels a) and c). Surface-normal sensible ( $H$ ) and latent heat ( $LE$ ) fluxes for panels b) and d).  
 329 Each point represents the hourly ensemble value for the fourth week of August 2010 ( $\pm$ SD). Open  
 330 symbols for panel b) represent points with <60% of data with quality flag "0" following Mauder and  
 331 Foken (2011).



332  
 333 **Fig 4** Energy balance closure for different energy sensor combinations: net radiation ( $R_n$ ), soil heat flux  
 334 ( $G$ ) and surface-normal sensible ( $H$ ) and latent ( $LE$ ) heat fluxes. Each point represents the hourly  
 335 ensemble value ( $H+LE$  vs.  $R_n+G$ ) for the entire measured period combining cloud-free and partially  
 336 cloudy days ( $\pm$ SD). Information about the slope, y-intercept and  $R^2$  is provided.



338

339 **Fig 5** Daily patterns of the energy balance components for different energy sensor combinations: net  
 340 radiation ( $R_n$ ), soil heat flux ( $G$ ) and surface-normal sensible ( $H$ ) and latent ( $LE$ ) heat fluxes. Each point  
 341 represents the hourly ensemble value of the different energy components for the entire measured period  
 342 combining cloud-free and partially cloudy days ( $\pm SD$ ). Open circles represent points with  $<60\%$  of data  
 343 with quality flag "0" following Mauder and Foken (2011).

344

345 **Acknowledgements** We wish to thank for their critical opinions and valuable comments that inspired this  
 346 manuscript: Edward Ayres, Robert Clement, Thomas Foken, Hongyan Luo, Harry McCaughey,  
 347 NatchayaPingingtha-Durden, and Jielun Sun. This research was funded in part by the Andalusia Regional  
 348 Government through projects P12-RNM-2409 and P10-RNM-6299, by the Spanish Ministry of Economy  
 349 and Competitiveness through projects CGL2010-18782, CGL2014-52838-C2-1-R (GEISpain) and  
 350 CGL2013-45410-R; and by European Community's Seventh Framework Programme through INFRA-  
 351 2010-1.1.16-262254 (ACTRIS), INFRA-2011-1-284274 (InGOS) and PEOPLE-2013-IOF-625988  
 352 (DIESEL) projects. The National Ecological Observatory Network is a project sponsored by the National  
 353 Science Foundation and managed under cooperative agreement by NEON, Inc. This material is based  
 354 upon work supported by the National Science Foundation under the grant DBI-0752017. Any opinions,  
 355 findings, and conclusions or recommendations expressed in this material are those of the author(s) and do  
 356 not necessarily reflect the views of the National Science Foundation.

357

### 358 **References**

359 Alados I, Foyo-Moreno, Alados-Arboledas L (2003) Relationship between net radiation  
 360 and solar radiation for semi-arid shrub-land. *Agric For Meteorol* 116(3–4):221-227  
 361 doi:10.1016/S0168-1923(03)00038-8

- 362 Aubinet M (2008) Eddy covariance CO<sub>2</sub> flux measurements in nocturnal conditions:  
 363 An analysis of the problem. *Ecol. Appl.* 18(6):1368-1378 doi: [http://dx.](http://dx.doi.org/10.1890/06-1336.1)  
 364 [doi.org/10.1890/06-1336.1](http://dx.doi.org/10.1890/06-1336.1)
- 365 Aubinet M, Berbigier P, Bernhofer CH, Cescatti A, Feigenwinter C, Granier A,  
 366 Grünwald TH, Havrankova K, Beinesch B, Longdoz B, Marcolla B, Montagnini L,  
 367 Sedlak P(2005) Comparing CO<sub>2</sub> storage and advection conditions at night at  
 368 different carboeuroflux sites. *Boundary-Layer Meteorol* 116(1):63-93  
 369 doi:10.1007/s10546-004-7091-8
- 370 Aubinet M, Grelle A, Ibrom A, Rannik Ü, Moncrieff J, Foken T, Kowalski AS, Martin  
 371 PH, Berbigier P, Bernhofer CH, Clement R, Elbers J, Granier A, Grünwald T,  
 372 Morgenstern K, Pilegaard K, Rebmann C, Snijders W, Valentini P, Vesla T (2000)  
 373 Estimates of the annual net carbon and water exchange of forests: the EUROFLUX  
 374 methodology. *Adv Ecol Res* 30:113-173
- 375 Aubinet M, Heinesch B, Yernaux M (2003) Horizontal and vertical CO<sub>2</sub> advection in a  
 376 sloping forest. *Boundary-Layer Meteorol* 108(3):397-417
- 377 Baldocchi DD, Falge E, Gu L, Olson R, Hollinger D, Running S, Anthoni P, Bernhofer  
 378 CH, David K, Evans R, Fuentes J, Goldstein A, Katul G, Law B, Lee X, Malhi Y,  
 379 Meyers Tm Paw U KT, Pilegaard K, Schmid HP, Valentini R, Verma S, Vesala T,  
 380 Wilson K, Wofsy S (2001) FLUXNET: A new tool to study the temporal and  
 381 spatial variability of ecosystem-scale carbon dioxide, water vapor, and energy flux  
 382 densities. *Bull Am Meteorol Soc* 82:2415–2434doi: [http://dx.](http://dx.doi.org/10.1175/1520-0477(2001)082<2415:FANTTS>2.3.CO;2)  
 383 [doi.org/10.1175/1520-0477\(2001\)082<2415:FANTTS>2.3.CO;2](http://dx.doi.org/10.1175/1520-0477(2001)082<2415:FANTTS>2.3.CO;2).
- 384 Domingo F, Villagarcia L, Brenner AJ, Puigdefábregas J (2000) Measuring and  
 385 modelling the radiation balance of a heterogeneous shrubland. *Plant Cell Environ*  
 386 23:27-38 doi: [10.1046/j.1365-3040.2000.00532.x](http://dx.doi.org/10.1046/j.1365-3040.2000.00532.x).
- 387 Etzold S, Buchmann N, Eugster W (2010) Contribution of advection to the carbon  
 388 budget measured by eddy covariance at a steep mountain slope forest in  
 389 Switzerland. *Biogeosci*7(8):2461-2475. doi:10.5194/bg-7-2461-2010.
- 390 Foken T (2008) The energy balance closure problem: an overview. *Ecol Appl*  
 391 18(6):1351-1367 doi: <http://dx.doi.org/10.1890/06-0922.1>.
- 392 Garnier BJ, Ohmura A (1968) A method of calculating the direct shortwave radiation  
 393 income of slopes. *J Appl Meteorol* 7(5):796-800doi:  
 394 [http://dx.doi.org/10.1175/1520-0450\(1968\)007<0796:AMOCTD>2.0.CO;2](http://dx.doi.org/10.1175/1520-0450(1968)007<0796:AMOCTD>2.0.CO;2).
- 395 Gu L, Falge EM, Boden T, Baldocchi D, Black TA, Saleska SR, Suni T, Verma SB,  
 396 Vesala T, Wofsy SC, Xu L (2005) Objective threshold determination for nighttime  
 397 eddy flux filtering. *Agric For Meteorol* 128:179-197  
 398 doi:10.1016/j.agrformet.2004.11.006.
- 399 Hammerle A, Haslwanter A, Schmitt M, Bahn M, Tappeiner U, Cernuscas A, Wohlfahrt  
 400 G (2007) Eddy covariance measurements of carbon dioxide, latent and sensible  
 401 energy fluxes above a meadow on a mountain slope. *Boundary-Layer Meteorol*  
 402 122(2):397-416 doi:10.1007/s10546-006-9109-x.
- 403 Hiller R, Zeeman MJ, Eugster W (2008) Eddy-covariance flux measurements in the  
 404 complex terrain of an alpine valley in Switzerland. *Bound-Layer Meteorol.*  
 405 127(3):449-467 doi:10.1007/s10546-008-9267-0.

- 406 Holst T, Rost J, Mayer H (2005) Net radiation balance for two forested slopes on  
 407 opposite sides of a valley. *Int J Biometeorol* 49(5):275-284 doi:10.1007/s00484-  
 408 004-0251-1.
- 409 Iqbal M (1983) *Introduction to solar radiation*. Academic Press, New York.
- 410 Kaminski T, Rayner PJ, Voßbeck M, Scholze M, Koffi E (2012) Observing the  
 411 continental-scale carbon balance: assessment of sampling complementarity and  
 412 redundancy in a terrestrial assimilation system by means of quantitative network  
 413 design. *Atmos Chem Phys* 12(16):7867-7879 doi:10.5194/acp-12-7867-2012.
- 414 Koffi EN, Rayner PJ, Scholze M, Chevallier F, Kaminski T (2013) Quantifying the  
 415 constraint of biospheric process parameters by CO<sub>2</sub> concentration and flux  
 416 measurement networks through a carbon cycle data assimilation system. *Atmos*  
 417 *Chem Phys* 13(21):10555-10572 doi:10.5194/acp-13-10555-2013.
- 418 Kowalski AS, Anthoni PM, Vong RJ, Delany AC, Maclean GD (1997) Deployment and  
 419 evaluation of a system for ground-based measurement of cloud liquid water  
 420 turbulent fluxes. *J Atmos Ocean Technol* 14:468-479
- 421 Kowalski S, Sartore M, Burllett R, Berbigier P, Loustau D (2003) The annual carbon  
 422 budget of a French pine forest (*Pinus pinaster*) following harvest. *Global Change*  
 423 *Biol* 9(7):1051-1065 doi: 10.1046/j.1365-2486.2003.00627.x.
- 424 Leuning, R, van Gorsel E, Massman WJ, Isaac PR (2012) Reflections on the surface  
 425 energy imbalance problem. *Agric For Meteorol* 156:65-74  
 426 doi:10.1016/j.agrformet.2011.12.002.
- 427 Massman WJ (1992) Correcting errors associated with soil heat flux measurements and  
 428 estimating soil thermal properties from soil temperature and heat flux plate data.  
 429 *Agric Forest Meteorol* 59(3-4):249-266 doi:10.1016/0168-1923(92)90096-M.
- 430 Matzinger N, Andretta M, van Gorsel E, Vogt R, Ohmura A, Rotach MW (2003)  
 431 Surface radiation budget in an Alpine valley. *Q J R Meteorol Soc* 129(588):877-  
 432 895 doi:10.1256/qj.02.44.
- 433 Mauder M, Foken T (2004) Documentation and instruction manual of the eddy-  
 434 covariance software package TK3. *Abt Mikrometeorologie* 46, 60 pp
- 435 McMillen R (1988) An eddy correlation technique with extended applicability to non-  
 436 simple terrain. *Boundary-Layer Meteorol* 43(3):231-245 doi: 10.1007/bf00128405.
- 437 Oliver HR (1992) Studies of surface energy balance of sloping terrain. *Int J Climatol*  
 438 12(1):55-68 doi: 10.1002/joc.3370120106
- 439 Olmo FJ, Vida J, Castro-Diez Y, Alados-Arboledas L (1999) Prediction of global  
 440 irradiance on inclined surfaces from horizontal global irradiance. *Energy* 24(8):689-  
 441 704 doi:10.1016/S0360-5442(99)00025-0.
- 442 Saitoh TM, Tamagawa I, Muraoka H, Koizumi H (2011) Energy balance closure over a  
 443 cool temperate forest in steeply sloping topography during snowfall and snow-free  
 444 periods. *J Agric Meteorol* 67(3):107-116 doi: 10.2480/agrmet.67.3.4.
- 445 Serrano-Ortiz P, Marañón-Jiménez S, Reverter BR, Sánchez-Castro EP, Castro J,  
 446 Zamora R, Kowalski AS (2011) Post-fire salvage logging reduces carbon  
 447 sequestration in Mediterranean coniferous forest. *Forest Ecol Manag* 262:2287-  
 448 2296 doi:10.1016/j.foreco.2011.08.023.

- 449 Shimizu T(2015) Effect of coordinate rotation systems on calculated fluxes over a forest  
 450 in complex terrain: a comprehensive comparison. *Boundary-Layer Meteorol*  
 451 156:277-301 doi: 10.1007/s10546-015-0027-7
- 452 Stoy P, Mauder M, Foken T, Marcolla B, Boegh E, Ibrom A, Altaf Arain M, Arneth A,  
 453 Aurela M, Bernhofer C, Cescatti A, Dellwik E, Duce P, Gianelle D, van Gorsel E,  
 454 Kiely G, Knohl A, Margolis H, MmCaughey H, Merbold L, Montagnani L, Papale  
 455 D, Reichstein M, Saunders M, Serrano-Ortiz P, Sottocornola M, Spano D, Vaccari  
 456 F, Varlagin A (2013) A data-driven analysis of energy balance closure across  
 457 FLUXNET research sites: The role of landscape-scale heterogeneity. *Agric For*  
 458 *Meteorol* 171-172:137-152.
- 459 Suyker AE, Verma SB (2001) Year-round observations of the net ecosystem exchange  
 460 of carbon dioxide in a native tallgrass prairie. *Global Change Biol* 7(3):279-289  
 461 doi: 10.1046/j.1365-2486.2001.00407.x.
- 462 Tanner BD, Thurtell GW (1969) Research and development technical report:  
 463 Anemoclinometer measurements of Reynold stress and het transport in the  
 464 atmopheric surface layer, University of Wisconsin, Wisconsin, Grant Number DA-  
 465 AMC-28-043-066-G022.
- 466 Turnipseed AA, Anderson DE, Blanken PD, Baugh WM, Monson RK (2003) Airflows  
 467 and turbulent flux measurements in mountainous terrain: Part 1. Canopy and local  
 468 effects. *Agric For Meteorol* 119(1–2):1-21. doi:10.1016/S0168-1923(03)00136-9
- 469 Webb EK, Pearman GI, Leuning R (1980) Correction of flux measurements for density  
 470 effects due to heat and water vapour transfer. *Q J R Meteorol Soc* 106(447):85-100  
 471 doi: 10.1002/qj.49710644707.
- 472 Whiteman CD, Allwine KJ, Fritschen LJ, Orgill MM, Simpson JR (1989) Deep valley  
 473 radiation and surface energy budget microclimates. Part I: Radiation. *J Appl*  
 474 *Meteorol* 28(6):414-426
- 475 Wilson K, Goldstein A, Flage E, Aubinet M, Baldocchi D, Berbigier P, Bernhofer C,  
 476 Ceulemans R, Dolman H, Field C, Grelle A, Ibrom A, Law BE, Kowalski A,  
 477 Meyers T, Moncrieff J, Monson R, Oechel W, Tenhunen J, Verma Sm Valentini R  
 478 (2002) Energy balance closure at FLUXNET sites. *Agric Fore Meteorol* 113(1–  
 479 4):223-243 doi:10.1016/S0168-1923(02)00109-0.
- 480 Wohlfahrt G,Tasser E (2014) A mobile system for quantifying the spatial variability of  
 481 the surface energy balance: design and application. *Int J Biometeorol*59:617-627  
 482 doi:10.1007/s00484-014-0875-8.
- 483 Zitouna-Chebbi R, Prévot L, Jacob F, Mougou R, Voltz M (2012) Assessing the  
 484 consistency of eddy covariance measurements under conditions of sloping  
 485 topography within a hilly agricultural catchment. *Agr Forest Meteorol* 164:123-  
 486 135.